# Near-field Radiation Patterns for an Ultra-Wide-Band Antenna

**Jonathan Blackledge*** **and Bazar Babajanov****

*School of Electrical and Electronic Engineering*
*Dublin Institute of Technology, Kevin Street, Dublin 8, Ireland*

E-mail: *jonathan.blackledge@dit.ie **a.murod@mail.ru

*Abstract* — **We present a three-dimensional time dependent model for simulating the electromagnetic radiation field patterns generated by Ultra-Wide-Band (UWB) antennas. UWB antennas are pulsed mode radiators used to communicate information at high bit rates over short distances. This affects the spatial characteristics of the field patterns assumed to be generated when a Continuous Wave (CW) model is used and this paper investigates the differences between the near-field intensity patterns generated when a pulse and CW mode is used. The purpose of this is to develop a numerical simulation that provides information on the three-dimensional electromagnetic field subject to a known (integrated) antenna geometry. The context of the approach considered is the design of integrated antennas that extend the performance of UWB systems in terms of range (in the near-field) subject to emission standards.**

*Keywords* — **lectromagnetic field patterns, time domain simulation, integrated Ultra-Wide-Band antennas, pulse mode signals.**

## I Introduction

Time-dependent analysis is important in the design of Ultra-Wide-Band (UWB) antennas which emit radio waves with a bandwidth exceeding 20% of the carrier frequency and operate in a frequency range from 3.1 to 10.6 GHz. The power spectral density emissions are limited to -41.3 dBm/MHz although they may be significantly lower (as low as -75 dBm/MHz) in other segments of the spectrum [1].

Due to the low emission levels permitted by regulatory agencies, UWB systems tend to be short-range indoor applications and are used to generate short pulse lengths enabling the transmission of high data rate signals. Due to the short duration of UWB pulses (less than 60 cm for a 500 MHz-wide pulse and less than 23 cm for a 1.3 GHz-bandwidth pulse), it is easy engineer high data rates (with a spatial capacity of approximately 1013 bits $s^{-1}m^{-2}$) which may be exchanged for range by aggregating pulse energy per data bit (with integration or coding techniques).

The Impulse Response Function (IRF) of a UBS antenna is typically given by a modulated Gaussian pulse and applications include high precision through-wall radar imaging using precision time-of-arrival-based localisation approaches and PC-peripherals such as wireless printers. In such cases, additional time domain analysis is necessary to characterise the antennas overall performance for pulsed signal transmission. Parameters such as pulse distortion and antenna fidelity need to be analysed together with standard antenna performance parameters for reliable design [2]

Simulating the three-dimensional field patterns generated by a continuous wave antenna radiating frequency or phase modulated narrow-band electromagnetic waves is a well known. The near-field scattering effect generated by integrated antennas used on mobile devices, for example, has also been investigated. Such simulations are important in evaluating the antenna design but are based on a time-independent analysis of the radiation field. Research has also been undertaken on simulating the time dependent behaviour of UWB pulses and the radiation field patterns generated in the far-field. In this paper we address the issue of developing a model to simulate the time-dependent,

near-field patterns associated with an integrated antenna in which interaction of the electromagnetic field occurs with the local environment into which the antenna is placed. In particular, we explore how the radiated field patterns change when a time-dependent solution to the problem is considered, a consequence of emitting a pulse rather than a continuous wave. This is important in terms of establishing the spatial intensity of the fields generated by UWB communication systems in order that antennas can be designed that are applicable over longer ranges subject to current emission standards.

In Section II, we consider an electromagnetic model and briefly review the basic homogenous material parameters associated with a conductive dielectric. Section III considers the solution methods associated with the general case. This provides the background to the analysis of a pulsed system given in Section IV which is the papers principal contribution to the field. Section V provides some example simulations comparing the near-field patterns for a continuous wave and a pulsed system associated with a simple monopole antenna.

## II Electromagnetic Model

It is well known that under the conditions of material linearity and isotropy, the three-dimensional, inhomogeneous scalar electric wavefield $u(\mathbf{r},k)$ (where $\mathbf{r}$ defines the three-dimensional space vector) is given by the solution to [3], [4]

$$(\nabla^2+k^2)u(\mathbf{r},k)=-\Gamma(\mathbf{r},k)u(\mathbf{r},k) \qquad (1)$$

where

$$\Gamma(\mathbf{r},k)=k^2(\epsilon_r-1)-ikz_0\sigma(\mathbf{r})$$

which is taken to be of compact support, i.e. $\Gamma\exists\forall\mathbf{r}\in\mathbb{R}^3$. In equation (1), $\epsilon_r$ is the relative permittivity, $\sigma$ is the conductivity, $k=2\pi/\lambda=\omega/c_0$ is the wavenumber defined for wavelength $\lambda$, angular frequency $\omega$ and speed of light in a vacuum $c_0$. The coefficient $z_0$ is the impedance of free space given by $z_0=\mu_0c_0\simeq 376:6$ Ohms where $\mu_0$ is the permeability of free space and $c_0=1/\sqrt{\epsilon_0\mu_0}$ where $\epsilon_0$ is the permittivity of free space.

Equation (1), is based on ignoring polarisation effects (with regard to the electric field) and assumes that the relative permeability is 1. It is also predicated on the validity of Ohm's law in which the electric field is given by the product of the conductivity $\sigma$ and the current density $j$, i.e. $j(\mathbf{r},k)=\sigma(\mathbf{r})u(\mathbf{r},k)$, which yields the term $ikz_0\sigma(\mathbf{r})$ in equation (1). The inhomogeneities in the relative permittivity and conductivity generates scattering effects especially when individual source-reflector components are used to contract the antenna and/or the antenna has a complex spatial topology. Based on equation (1), this paper focuses of modelling this effect for a continuous wave and a pulse of electromagnetic radiation generated by a primary source (an antenna) located in the vicinity of a conductive dielectric, a scenario that is consistent with an integrated antenna.

*a) Homogeneous Properties*

For the homogenous case, when $\epsilon_r(\mathbf{r})=1$ and $\sigma(\mathbf{r})=\sigma_0,\ \ \forall\mathbf{r}\in\mathbb{R}^3$, equation (1) reduces to

$$(\nabla^2+k^2+ikz_0\sigma_0)u(\mathbf{r},k)=0 \qquad (2)$$

which (for a unit vector $\hat{\mathbf{n}}$) has a simple 'plane wave solution' of the form

$$u(\mathbf{r},k)=\exp(\pm iK\hat{\mathbf{n}}\cdot\mathbf{r}),\quad K=k\sqrt{1+iz_0\sigma_0/k}$$

Thus, when $\sigma_0/k>>1$, and noting that $K\simeq\sqrt{ikz_0\sigma_0}=(1+i)\sqrt{kz_0\sigma_0/2}$, we obtain the physically significant result (i.e. the wave amplitude cannot increase indefinitely)

$$u(\mathbf{r},k)=\exp(i\sqrt{kz_0\sigma_0/2}\hat{\mathbf{n}}\cdot\mathbf{r})\exp(-\sqrt{kz_0\sigma_0/2}\hat{\mathbf{n}}\cdot\mathbf{r})$$

which yields a solution with a negative exponential decay characterised by the skin depth

$$\delta=\sqrt{2/kz_0\sigma_0}$$

Further, if the absorption characteristics of the medium are taken to be determined from the solution (for real $K$)

$$u(\mathbf{r},k)=\exp(iK\hat{\mathbf{n}}\cdot\mathbf{r})\exp(-\alpha\hat{\mathbf{n}}\cdot\mathbf{r})$$

then, from equation (2), we obtain

$$-(K+i\alpha)^2+k^2+ikz_0\sigma_0=0$$

so that, upon equating real and imaginary parts,

$$\alpha=\frac{k}{\sqrt{2}}\left[\left(1+\frac{z_0\sigma_0^2}{k^2}\right)^{\frac{1}{2}}-1\right]^{\frac{1}{2}}$$

The phase velocity is given by $2\alpha/\mu_0\sigma_0$ and we note that when $z_0\sigma_0/k<<1$, $\alpha=z_0\sigma_0/2$, the absorption characteristics are independent of wavelength and the phase velocity is $c_0$.

The Green's function for this medium, i.e. the idealised IRF given by the solution to the equation

$$(\nabla^2+k^2+ikz_0\sigma_0)g(r,k)=-\delta^3(\mathbf{r}),\quad r\equiv\mid\mathbf{r}\mid$$

where $\delta^3$ denotes the three-dimensional delta function, is [3]

$$g(r,k)=\frac{1}{4\pi r}\exp(i\sqrt{k^2+ikz_0\sigma_0}r)$$

This function has the time-dependent form (for $tc_0>r$),

$$G(r,t)=-\frac{c_0}{4\pi r}$$
$$\times\exp(-z_0\sigma_0c_0^2t/2)\frac{\partial}{\partial r}\left[I_0\left(\frac{z_0\sigma_0c_0}{2}\sqrt{c_0^2t^2-r^2}\right)\right]$$

where $I_0$ is the modified Bessel function of order zero.

*b) Field Generated by a Conductive Source*

For a conductive source $\epsilon_r = 1$ and we obtain the following Green's function solution to equation (1) subject to 'homogenous boundary conditions' [3]

$$u(\mathbf{r}, k) = ikz_0 g(r, k) \otimes_{\mathbf{r}} j(\mathbf{r}, k) \tag{3}$$

where

$$g(r, k) = \frac{\exp(ikr)}{4\pi r}$$

which is the solution of

$$(\nabla^2 + k^2)g(r, k) = -\delta^3(\mathbf{r})$$

Here, $\otimes_{\mathbf{r}}$ denotes the three-dimensional convolution integral over $\mathbf{r}$ which, for two functions $f_1(\mathbf{r})$ and $f_2(\mathbf{r})$ (that may be both piecewise continuous and generalised functions), is defined as

$$f_1 \otimes_{\mathbf{r}} f_2 = \int_{\mathbb{R}^3} f_1(\mathbf{r}_0 - \mathbf{r}) f_2(\mathbf{r}) d^3\mathbf{r},$$

where, on a physical basis, $\mathbf{r}_0$ is the 'observation position'. Equation (3) gives the magnetic field generated by the current density $j$, and, under the scalar theory considered, is analogous to the computation of the Magnetic Vector Potential $\mathbf{M}$ from the current vector density $\mathbf{j}$ given by [3]

$$\mathbf{M}(\mathbf{r}, k) = \mu_0 g(r, k) \otimes_{\mathbf{r}} \mathbf{j}(\mathbf{r}, k)$$

and, for a pulsed system, yields the retarded potential

$$\mathbf{M}(\mathbf{r}_0, t) = \frac{\mu_0}{4\pi} \int_{\mathbb{R}^3} \mathbf{j}(\mathbf{r}, t + \mid \mathbf{r} - \mathbf{r}_0 \mid /c_0) d^3\mathbf{r}$$

The far-field patterns associated with this solution are considered in [5]. In this paper, we consider the near-field emission associated with the solution to equation (1). In principal, this allows variations in the conductivity and the relative permittivity to be considered over a region of space in which scattering effects are taken into account, a scenario which is compatible with the issue of simulating the radiation field pattern generated by an integrated antenna in which the proximity of the source to other dielectric components generates a scattering effects in both the near and far field.

## III Scattered Field Generated by a Conductive Dielectric

Consider the electromagnetic field $u$ to be given by the sum of some incident field $u_i$ emitted by the primary source of the antenna and a scattered field $u_s$, i.e. $u = u_i + u_s$. Noting that

$$\nabla^2 \frac{1}{4\pi r} = -\delta^3(\mathbf{r})$$

then

$$(\nabla^2 + k^2)u_s(\mathbf{r}, k) = \nabla^2 \left( u_s - \frac{k^2}{4\pi r} \otimes_{\mathbf{r}} u_s \right)$$

and equation (1) can be written in the form of the inhomogeneous Poisson equation

$$\nabla^2 \left[ u_s(\mathbf{r}, k) - \frac{k^2}{4\pi r} \otimes_{\mathbf{r}} u_s(\mathbf{r}, k) \right]$$

$$= -\Gamma(\mathbf{r}, k) u_i(\mathbf{r}, k) - \Gamma(\mathbf{r}, k) u_s(\mathbf{r}, k)$$

which has the Green's function solution

$$\left[ u_s(\mathbf{r}, k) - \frac{k^2}{4\pi r} \otimes_{\mathbf{r}} u_s(\mathbf{r}, k) \right]$$

$$= \frac{1}{4\pi r} \otimes_{\mathbf{r}} \Gamma(\mathbf{r}, k) u_i(\mathbf{r}, k) + \frac{1}{4\pi r} \otimes_{\mathbf{r}} \Gamma(\mathbf{r}, k) u_s(\mathbf{r}, k)$$

Collecting like terms, we have

$$u_s(\mathbf{r}, k) = \frac{1}{4\pi r} \otimes_{\mathbf{r}} \Gamma(\mathbf{r}, k) u_i(\mathbf{r}, k)$$

$$+ \frac{1}{4\pi r} \otimes_{\mathbf{r}} [k^2 + \Gamma(\mathbf{r}, k)] u_s(\mathbf{r}, k)$$

so that when $r_0 >> r$

$$u_s(\mathbf{r}_0, k) = \frac{c}{4\pi r_0} \int_{\mathbb{R}^3} \Gamma(\mathbf{r}, k) u_i(\mathbf{r}, k) d^3\mathbf{r} \tag{4}$$

where

$$c = \left( 1 + \frac{1}{4\pi r_0} \int_{\mathbb{R}^3} [k^2 + \Gamma(\mathbf{r}, k)] d^3\mathbf{r} + ... \right)$$

under the convergence condition

$$\frac{1}{4\pi r_0} \left| \int_{\mathbb{R}^3} [k^2 + \Gamma(\mathbf{r}, k)] d^3\mathbf{r} \right| < 1$$

If the source of the incident radiation is taken to in the far-field then $u_i$ can be considered to be a plane wave, but in the near field we can not assume the incidence of a plane wave front. We therefore consider the incident field to be given by the 'Fresnel zone Green's function' [3]

$$g(\mathbf{r}, \mathbf{r}_0, k) = \frac{1}{4\pi r_0} \exp(ikr_0) \exp(-ik\hat{\mathbf{n}} \cdot \mathbf{r}) \exp(i\alpha r^2)$$

where $\alpha = k/2r_0$. Equation (4) then becomes

$$u_s(\mathbf{r}_0, k) = c(r_0, k) \frac{\exp(ikr_0)}{(4\pi r_0)^2}$$

$$\times \int_{\mathbb{R}^3} \Gamma(\mathbf{r}, k) \exp(-ik\hat{\mathbf{n}} \cdot \mathbf{r}) \exp(i\alpha r^2) d^3\mathbf{r}$$

However, noting that

$$\frac{ik}{2r_0} \mid \mathbf{r}_0 - \mathbf{r} \mid^2 = \frac{ik}{2r_0}(r_0^2 + r^2 - 2\mathbf{r}_0 \cdot \mathbf{r})$$

$$= \frac{ikr_0}{2} + \frac{ikr^2}{2r_0} - ik\hat{\mathbf{n}} \cdot \mathbf{r}$$

we can write this result in the form

$$u_s(\mathbf{r}, \mathbf{r}_0, k) = c(r_0, k)\frac{\exp(ikr_0/2)}{(4\pi r_0)^2}A(\mathbf{r}, k)$$

where $A$ is the scattering amplitude function given by

$$A(\mathbf{r}, k) = \Gamma(\mathbf{r}, k) \otimes_{\mathbf{r}} \exp(i\alpha r^2) \tag{5}$$

the function $\exp(i\alpha r^2)$ being the (three-dimensional) Fresnel Point Spread Function (PSF). If this function is taken to be a source, then in the far-field, the intensity of the field is given by

$$I(\hat{\mathbf{n}}.k) = \mid \widetilde{A}(\hat{\mathbf{n}}, k) \mid^2$$

where

$$\widetilde{A}(\hat{\mathbf{n}}, k) = \int_{\mathbb{R}^3} A(\mathbf{r}, k)\exp(-ik\hat{\mathbf{n}} \cdot \mathbf{r})d^3\mathbf{r}, \quad \hat{\mathbf{n}} = \frac{\mathbf{r}_0}{r_0}$$

For a Continuous Wave (CW) system (subject to some modulation scheme) $k$ can be taken to be a constant.

## IV Pulsed Systems Analysis

For a pulsed system, $k$ has a side-band spectrum characterised by a Transfer Function $P(k)$ with carrier frequency $k_0$ and bandwidth $\Omega/c_0 << k_0$. Given equation (5), the near-field scattering amplitude now becomes

$$A(\mathbf{r}, k) = P(k)\Gamma(\mathbf{r}, k_0) \otimes_{\mathbf{r}} \exp\left(\frac{ikr^2}{2r_0}\right)$$

where $k \in [-\Omega/2c_0, \Omega/2c_0]$. Note that $\Gamma$ is taken to be a function of the carrier frequency alone since, unlike a base-band system, in a side-band system, the bandwidth is not significant enough for the spectral characteristics of the scattering function to be influential and $\Gamma(\mathbf{r}, k) \simeq \Gamma(\mathbf{r}, k_0)$. This is not the case for the complex exponential function since small changes in $k_0$ (i.e. perturbations to the carrier frequency within the bandwidth of the Transfer Function) can cause this function to change significantly (oscillate rapidly) particularly for large values of $r^2/2r_0$.

Using the convolution theorem, we now obtain

$$a(\mathbf{r}, \xi) = \frac{\Omega}{c_0}\text{sinc}\left(\frac{\Omega\xi}{2c_0}\right) \otimes_\xi p\left(\xi + \frac{r^2}{2r_0}\right) \otimes_{\mathbf{r}} \Gamma(\mathbf{r}, k_0) \tag{6}$$

where

$$a(\mathbf{r}, \xi) = \frac{1}{2\pi}\int_{-\infty}^{\infty} A(\mathbf{r}, k)\exp(ik\xi)dk,$$

$$p(\xi) = \frac{1}{2\pi}\int_{-\infty}^{\infty} P(k)\exp(ik\xi)dk$$

and $\otimes_\xi$ denotes the convolution integral over length $\xi = tc_0$. However, we can now exploit the fact that the pulse length $cT$ is generally much larger the dimensions of the antenna $L$ say so that

$$Tc_0 >> \frac{L^2}{2r_0}$$

which allows us, through Taylor expansion of the function $p$, i.e.

$$p\left(\xi + \frac{r^2}{2r_0}\right) \simeq p(\xi) + \frac{r^2}{2r_0}\frac{d}{d\xi}p(\xi)$$

to write equation (6) in the form

$$a(\mathbf{r}, \xi) = \frac{\Omega}{c_0}\text{sinc}\left(\frac{\Omega\xi}{2c_0}\right) \otimes_\xi ...$$

$$... \left[p(\xi)\bar{\Gamma}(k_0) + \frac{d}{d\xi}p(\xi)\frac{r^2}{2r_0} \otimes_{\mathbf{r}} \Gamma(\mathbf{r}, k_0)\right] \tag{7}$$

where

$$\bar{\Gamma}(k_0) = \int_{\mathbb{R}^3} \Gamma(\mathbf{r}, k_0)d^3\mathbf{r}$$

and $\otimes_\xi$ is now taken to be the convolution integral for $t \in [-Tc_0/2, Tc_0/2]$.

Equation (7) reveals that the pulse generated by a UWB antenna (given the model being considered) includes a second component determined by the first derivative of this pulse. However, in the context of the problem considered in this paper, the field pattern is determined by the convolution with $r^2$ which yields a very different result to the CW case. Comparing equations (6) and (7) we have

Near-field Wave Amplitude

$$= \begin{cases} \Gamma(\mathbf{r}, k_0) \otimes_{\mathbf{r}} \exp\left(i\frac{k_0 r^2}{2r_0}\right), & \text{CW System;} \\ P(k)\Gamma(\mathbf{r}, k_0) \otimes_{\mathbf{r}} i\frac{kr^2}{2r_0}, & \text{Pulsed System.} \end{cases} \tag{8}$$

where we have used the result ($\leftrightarrow$ being used to denote a Fourier transform pair)

$$\frac{d}{d\xi}p(\xi) \leftrightarrow ikP(k) \simeq ik_0P(k)$$

Similarly, in the far-field, we have

Far-field Wave Amplitude

$$= \begin{cases} \int\limits_{\mathbb{R}^3} \Gamma(\mathbf{r}, k_0) \exp(-ik_0 \hat{\mathbf{n}} \cdot \mathbf{r}) d^3\mathbf{r}, & \text{CW System;} \\ P(k) \int\limits_{\mathbb{R}^3} \Gamma(\mathbf{r}, k_0)(-ik\hat{\mathbf{n}} \cdot \mathbf{r}) d^3\mathbf{r}, & \text{Pulsed System.} \end{cases}$$

where, in the latter case, $Tc_0 >> L$. However, if the near-field wave amplitude is considered to be generated by near-field scattering effects due to the proximity of the primary source to other conductive dielectric components (as in an integrated antenna), then equation (8) defines the resultant source of radiation. The far-field wave amplitude is then given by the three-dimensional Fourier transform of this resultant near-field wave amplitude.

The (spatial) spectral properties of equation (8) exhibit significant differences between CW and pulse systems. Noting that (for an arbitrary real constant $a$)

$$\exp(iar^2) \leftrightarrow \left(\frac{\pi}{ia}\right)^{\frac{3}{2}} \exp\left(\frac{ik^2}{4a}\right)$$

and using the convolution theorem, the CW Transfer Function $T(\mathbf{k})$ of the near-field wave amplitude is

$$T_{\text{CW}}(\mathbf{k}) = \left(\frac{2\pi r_0}{ik_0}\right)^{\frac{3}{2}} \exp\left(\frac{ir_0 k^2}{2k_0}\right) \qquad (9)$$

The pulse Transfer Function can be approximated under the assumption that $k_0 r^2/2r_0 << 1$ so, given that,

$$\exp\left(\frac{ik_0 r^2}{2r_0}\right) \simeq 1 + \frac{ik_0 r^2}{2r_0}$$

we can write

$$T_{\text{Pulse}}(\mathbf{k}) \simeq -\delta^3(\mathbf{k}) + \left(\frac{2\pi r_0}{ik_0}\right)^{\frac{3}{2}} \exp\left(\frac{ir_0 k^2}{2k_0}\right) \qquad (10)$$

which shows that, relative to the CW case, i.e. equation (9), the spectrum is dominated by the DC component, compounded by the presence of the three-dimensional delta function $\delta^3$ given in equation (10). We should therefore expect the near-field radiation field for a pulsed system to be more uniformly distributed compared to the CW case. This is borne out in the example simulations that follow.

## V Simulation

We consider simulating of near-field wave amplitude using a three-dimensional $N^3$ regular Cartesian mesh based on the results given in equation (8). The function $k_0 r^2/2r_0$ can be scaled using the 'quarter wavelength resonance frequency condition'. Under this condition, we require the size of the antenna to be approximately one quarter of a wavelength and thus, within the domain of the convolution integrals $\mathbb{R}^3$, we let

$$\frac{\lambda}{4} \sim \Delta N$$

where $\Delta$ defines the spatial resolution of the mesh, the length of each side of a Voxel (Volume Element) being taken to be given by $\Delta$. In this case,

$$\frac{k_0 r^2}{2r_0} = \frac{\pi}{\lambda r_0} \Delta^2 (n_x^2 + n_y^2 + n_z^2)$$

where $n_x$, $n_y$, and $n_z$ are array indices running from $-N/2$ through 0 to $N/2$, the convolution given in equation (8) being computed over all space and not just the positive half-space. It is then clear that we obtain a wavelength independent (a consequence of the resonance condition) expression for $k_0 r^2/2r_0$, i.e.

$$\frac{k_0 r^2}{2r_0} = \frac{\pi}{4N} \frac{\Delta}{r_0} (n_x^2 + n_y^2 + n_z^2) \qquad (11)$$

where the numerical value for $\Delta/r_0$ must be (user) defined. Note that for a pulsed system, the resonance wavelength is taken to be the wavelength of the carrier frequency. The three-dimensional convolution sums required to implement results given in equation (8) are computed using the MATLAB function *convn* with the option 'same' which returns the central part of the convolution that is the same size as the input arrays.

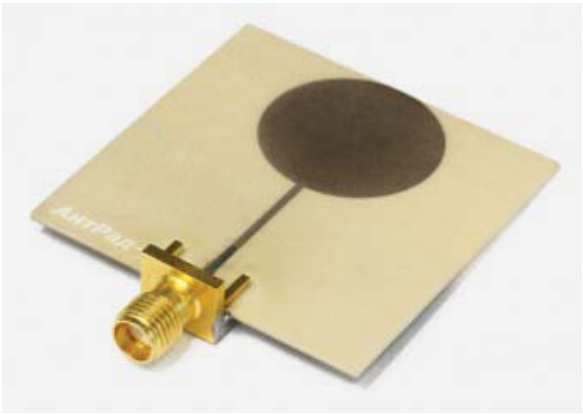

Fig. 1: Example of a UWB monopole antenna based on [6].

By way of an example, we consider a monopole UWB antenna of the type illustrated in Figure 1 [6] which is composed of a circular conductive element (with a connecting feed) mounted on a dielectric insulating slab. In general, the relative permittivity of the dielectric is not significant enough to contribute to the field pattern for the radio frequency range being considered when, for a 10 GHz system with a wavelength of 0.03m, and, for a metallic conductor $\sim 10^7$ siemens per metre, $k_0^2(\epsilon_1 - 1) << k_0 z_0 \sigma$ and $\Gamma \simeq ikz_0\sigma$.

The simulated field patterns are visualised using normalised intensity maps and hence, the complex coefficient $ikz_0$ and the physical value of the conductivity is not significant. Figure 2 shows an idealised representation of the monopole UWB antenna given in Figure 1 using a $100^3$ Voxel array. Voxels representing conductive elements are assigned a value of 1 and taken to have a thickness of 1 Voxel. The dielectric mount is also taken to have a thickness of 1Voxel. The element is taken to radiate an electric wavefield whose CW and pulsed field patterns are determined by equation (8) subject to equation (11). The intensity maps in the z-plane at $z = 2L$ are shown in Figure 3 for $\Delta/r_0 = 0.1$ which compares the near-field patterns in this plane for a continuous wave and a pulse associated with the configuration shown in Figure 2.

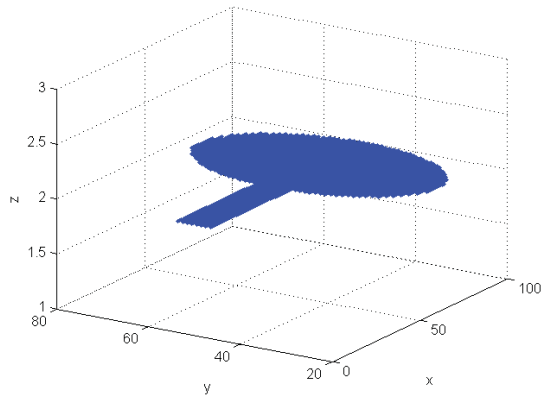


Fig. 2: Geometry of the monopole antenna illustrated in Figure 1 consisting of a single circular element and connecting feed taken to be mounted on a dielectric slab each with a thickness of 1 Voxel using a $100^3$ Cartesian mesh.

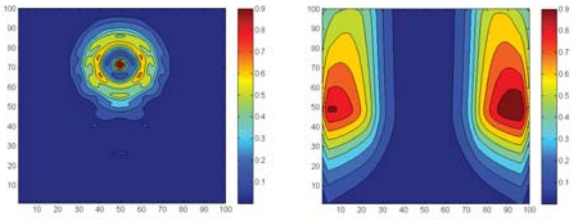

Fig. 3: Normalised near-field intensity maps in the plane at $z = 2L$ for a continuous wave (left) and a pulse (right) with $\Delta/r_0 = 0.1$.

This simulation provides a result that is compatible with a 'source only' solution which is compatible with the conventional computation of the Magnetic Vector Potential from the current density. However, within the context of equation (8) and the derivation thereof, we can extend the simulation to include the case of a source-reflector system as shown in Figure 4 where the dielectric is taken to be 'sandwiched' between the same monopole antenna and a reflector composed of material with the same conductivity, the antenna, dielectric and reflector each having a thickness of 1 Voxel.

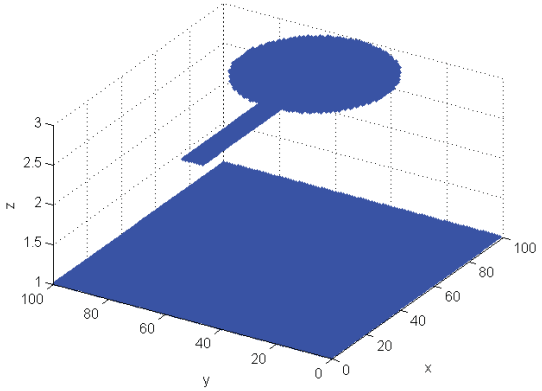


Fig. 4: Three-dimensional geometry of a monopole source-reflector system using a $100^3$ Cartesian mesh.

In this case, these field patterns are based on the scattering effects generated between the primary radiation source and the reflector. The scattered wavefield generated within $\mathbb{R}^3$ establishes a secondary radiation source which is 'plotted' as an intensity map in the z-plane at $z = 2L$ as shown in Figure 5. As expected from the analysis of the Transfer Functions given by equations (9) and (10), Figures 3 and 5 illustrate that, for a pulsed system, the radiation field is more uniformly distributed in comparison to the CW case. This is due to the lack of spatial coherence associated with a pulsed system given the model compounded in equation (8) where, in contrast to the CW case, there is no (quadratic) phase effect generated by convolution of the 'scattering function' with the Fresnel Point Spread Function $\exp(ik_0r^2/2r_0)$. In turn, this is a consequence of the pulse length being taken to by significantly larger than the dimensions of the antenna thereby facilitating a Taylor series approximation to the pulse function $p$ (under translation) given in equation (6).

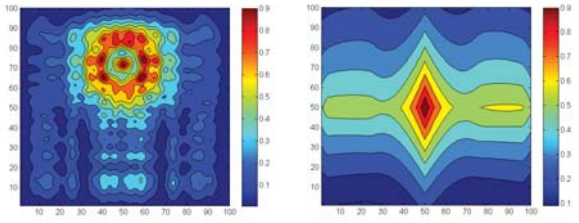

Fig. 5: Normalised near-field intensity maps in the plane at $z = 2L$ for a continuous wave (left) and a pulse (right) with $\Delta/r_0 = 0.1$.

## VI Conclusions

This paper has focused on provided a model for computing the near-electromagnetic field pattern generated by a UWB antenna. The model, which is compounded in equation (8), provides solutions for both CW and pulsed systems. The Transfer Functions for each case, and, as given by equations (9) and (10), illustrate a significant difference in the spatial frequency spectrum which, in the case of a pulse, is dominated by the DC component. Example simulations have been provided which illustrate these differences for a case study involving a monopole antenna with and without a reflector. The simulator can be used to characterise the CW/pulsed field patterns generated by a range of antenna geometries, e.g. [7] [8], [9], [10] and [11].

The principal contribution to the field has been to consider a three-dimensional model which incorporates the ability to model a single source (the conventional approach for computing the Magnetic Vector Potential as considered in [5], for example, and references therein) and a source-reflector system in a unified way, subject to the conditions required to consider a scalar Helmholtz scattering model, i.e. equation (1). However, subject to the conditions of linearity and material isotropy, the same approach can be used to evaluate the electric field subject to polarisation effects using the method given in [3], for example, which evaluates the scattering of a polarised microwave fields from a rough surface and is directly applicable to characterising UWB monopole and dipole antennas [11]. For readers interested in evaluating the numerical simulations provided in this paper and extending method further, a prototype m-code function is available from [12].

## Acknowledgements

Jonathan Blackledge is supported by the Science Foundation Ireland Stokes Professorship Programme. Dr Bazar Babajanov is supported by the Erasmus Mundus Action II co-operation and the mobility programme EASTANA (EuroAsian Starter for Technical Academic Network Applications).

## References

[1] Federal Communications Commission FCC 02-48, "Revision of Part 15 of the Commission's Rules Regarding Ultra-Wide-Band Transmission Systems", April 22, 2002, available online from: http://hraunfoss.fcc.gov/edocs_public/attachmatch/FCC-02-48A1.pdf.

[2] Time Analysis of UWB Antennas, 2013, available online from: http://www.feko.info/applications/white-papers/time-analysis-of-UWB-antenna/uwb-monopole-antenna

[3] J. M. Blackledge, *Digital Image Processing*, Horword Publishing, 2005.

[4] J. M. Blackledge, M. Ammann, B. Babajanov and A. Panahi, "Three-dimensional Simulation of the Radiation Field Patterns Generated by an Integrated Antenna", IJAM International Journal of Applied Mathematics, (Submitted), 2013.

[5] A. Shlavinski, E. Heyman and R. Kastner, "Antenna Characterisation in the Time Domain", IEEE Transactions on Antennas and Propagation Vol. 45, No. 7, pp. 1140-1149, 1997.

[6] UWB antenna Antrad-4, 3-10 GHz, 2013, available online from: http://uwbs.ru/en/products/sverhshirokopolosnye-pechatnye-i-rupornye-antenny/sverhshirokopolosnaya-antenna-antrad4/

[7] L. C. Kuo, M. C. Tsai and H. R. Chuang, "3D FDTD Design Simulation and Experimental Measurement of a Ka-band Planar Antipodal Linearly-Tapered Slot Antenna (ALTSA), IEEE Guidedwave & Wireless Components Letter, Vol. 11, No. 9, pp. 382?84, 2001.

[8] S. B. Chen, Y. C. Jiao, W. Wang and Q. Z. Liu, "Wideband CPW-fed Uniplanar Sleeve-Shaped Monopole Antenna, Microwave Opt. Technol. Lett., Vol. 47, No. 3, pp. 245-47, 2005.

[9] K. H. Kim and and S. O. Park, "Analysis of the Amall Band-rejected Antenna with the Parasitic Strip for UWB, IEEE Trans. Antennas Propagation, Vol. 54, pp. 1688?692, 2006.

[10] C. C. Lin, H. R. Chuang and Y. C. Kan, "A 2-12GHz UWB Planar Triangular Monopole Antenna with Rudges Ground Plate, Progress In Electromagnetics Research, PIER 83, pp. 307?21, 2008.

[11] H. N. Lin, C. M. Shao and J. L. Chen, "Design of Ultra-wideband Monopole Antenna with Band-notched and GPS Circular Polarization Characteristics Progress In Electromagnetics Research Symposium, Hangzhou, China, March 24-28, pp. 151-156 2008.

[12] J. M. Blackledge, *m-code for function UWBFPS.m*, available online from: http://eleceng.dit.ie/jblackledge/ISS2013.zip